Magazine of Civil Engineering

ISSN 2712-8172

journal homepage: http://engstroy.spbstu.ru/

DOI: 10.18720/MCE.99.10

Behavior of B-C connections damaged by thermal shock

R. Al-Rousan*
Jordan University of Science and Technology, Irbid, Jordan
** E-mail: rzalrousan@just.edu.jo*

Keywords: reinforced concrete, thermal shock, structural strength, horizontal load, fiber reinforced polymer, nonlinear, finite element analysis.

Abstract. The behavior of beam-column (B-C) connections received thorough investigation during the past decades focusing on critically-detailed connections before and after strengthening. Exposure of such B-C connections to thermal shock due to subjected to cycles of heating–cooling such as in chimneys, concrete foundations for launching rockets carrying spaceships, concrete near to furnace, clinker silos and nuclear power plants, or those subjected to fire then extinguished using water would aggravate the weakness of the high joint zone. In this study, systematic nonlinear finite element analyses (NLFEA) were conducted using ANSYS to evaluate the effects of the level of the column axial load and thermal shock impact which is a parameter difficult to evaluate experimentally due to limitations in loading machines and requirement for complicated testing setups. A total of eight NLFEA models were created, calibrated and properly verified with reputable experimental literature results. The NLFEA results showed that both level of the column axial load and thermal shock impact significantly affect the cracks distribution, failure mode, ultimate load capacity, and ductility of the B-C connection. Column axial load levels up to 75 % were advantageous to the behavior of virgin B-C connections. The lateral load capacities, net drifts, hysteresis loops, cracks distribution, energy dissipation, and failure modes were presented.

1. Introduction

One of the main reasons for collapsing of reinforced concrete frame structures is the failure of the B-C connections by shearing of the joint or column. Critical beam-column (B-C) connection details common in buildings constructed before 1970s and still used in third-world countries include: discontinuous bottom beam reinforcement, lap-splicing of the column bars just above the joint, and lack of joint confinement. Proper strengthening of the B-C joint results in improved structural behavior and failure mode transformation [1]. Failure of the joint or the column is sudden and accompanied with low ductility and energy dissipation. It leads to dangerous local collapses that may cause progressive total collapse of the structure. The other failure mode is a desired ductile one in the beam typically at short distance from the face of the column. It is important when analyzing the B-C connections to consider all the aforementioned failure modes.

Recent studies focused on creating numerical simulations and modeling of the B-C joint under seismic loading. Researchers proposed three types of B-C joint models such as: rotational hinge models [2]; component models [3–5], and nonlinear finite element analysis (NLFEA) [6]. Each model has advantages and limitations, and there is no scientific agreement on a model that is optimal for all applications. However, NLFEA that takes into consideration materials and geometric nonlinearities provides accurate results if properly simulated, calibrated, and validated with reputable experimental results. It also saves tremendous amount of time and cost compared with experimental testing [6–7]. Using a strut-and-tie model, Sasmal et al. [8] found that most of the energy was dissipated through the development of damage in the joint region, which not safe for the stability of the entire structure. Venkatesana et al. [6] carried out experimental tests and numerical simulations using ANSYS software for the seismic performance of exterior B-C joints before and after strengthening with ferrocement jackets, and found that the analytical shear strength predictions were in line with the test results. Sasmal and Nath [7] introduced a steel bracing technique to strengthen poorly designed B-C joints, and their NLFEA using ATENA package demonstrated the improvement in crack patterns, ultimate load, energy dissipation, and ductility after strengthening. Lima et al. [9] modeled the exterior B-C joints as nonlinear rotational spring elements, and their results confirmed that neglecting the effects of joints damage

might potentially lead to non-conservative seismic assessment of existing reinforced concrete framed structures. Ibrahim et al. [10] carried out finite element modeling of exterior beam-column joints strengthened by ferrocement under cyclic loading found that the effect of orientation angle became less significant on the ductility with increasing the number of ferrocement layers used for strengthening. More recent studies were published [11–14] and provided good information toward better understanding of the behavior of the B-C joints, which considered essential for future calibration of the design codes as well as repairing techniques.

Elevated temperatures cause severe damage for reinforced concrete (RC) structures, such as RC beams. RC beams have been reported to loss strength and stiffness with relatively large permanent deformations because of exposure to high temperatures [15]. These harmful effects could be attributed to the deterioration of mechanical characteristics of concrete and steel rebars and the redistribution of stresses within the beam due to the elevated temperatures [15, 16]. Currently, the most used technique to repair the heat-damaged RC beams is using carbon fiber reinforced polymer (CFRP) composites. These sheets are advanced materials that can be easily applied on the structures and characterized by outstanding mechanical and corrosion resistance characteristics. Various studies were performed to investigate the flexural behavior of RC beams wrapped with CFRP. The results showed that externally bonded carbon FRP (CFRP) sheets and laminates can enhance the flexural behavior of the beams and recover, to certain limit, the flexural strength of heat-damaged beams. Strengthening level or recovery depends on several factors such as fire resistance [17], elevated temperature [18, 19], fiber type [20–23], analysis type [24–28], energy integrity resistance [29], anchored system [30], heating condition [31–33], degree of beam's damage and geometry and type of fiber sheet [34], and safety factors for CFRP strengthening of bridges [35].

Reinforcing concrete structures are often subjected to cycles of heating–cooling such as in chimneys, concrete foundations for launching rockets carrying spaceships, concrete near to furnace, clinker silos and nuclear power plants, or those subjected to fire then extinguished using water. Temperature cycles are critical to the stability of concrete structures and require considerations upon design [36, 37]. As well stipulated, the mechanical properties of concrete are preserved for exposure temperatures below 300 °C, yet are decreased considerably as temperature exceeds 500 °C. Additional damage results from rabid cooling such as in the case of distinguishing of fire with cool water due to creation of temperature gradient between concrete core and its surface. This results in tensile stresses on the concrete surface that are high enough to crack concrete and this considered as another source of damage results from incompatible expansion and contraction of aggregate and surrounding cement paste. The magnitude of damage is influenced by many factors such as the size of concrete members, the type of cement and aggregate, the concrete moisture content and the predominant environmental factors, Those are represented in heating exposure time and rate, type of cooling, and maximum temperature attained [38]. Different types of materials and techniques were used in strengthening and retrofitting of existing concrete structures such as steel plates bolting, reinforced concrete jackets, pre-stressed external tendons, and most recently FRP composite which has been used on a large scale in different countries. FRP composites have many advantages over conventional methods represented in ease of application, high strength-to-weight ratio, excellent mechanical strength, and good resistance to corrosion, especially that most structures are damaged due to dynamic loads, corrosion of steel, and freeze-thaw cycles [39, 40].

Many reinforced concrete bridges are deteriorating due to problems related to environment and increase in load of trucks. Also, the impact of thermal shock on the behavior of deficient reinforced concrete B-C connections must receive miniature consideration. The scientific problem considered in the study is indeed one of the problems in the modern theory of deficient reinforced concrete B-C connections. A lack of literature regarding behavior of deficient columns damaged by thermal shock necessitated conducting the present investigation. In this study, NLFEA program were carried out to find the improvements in the strength and ductility behavior of reinforced concrete (RC) B-C connections damaged by thermal shock. This parametric study provides systematic nonlinear FEA using ANSYS software addressing key parameters related to the behavior of B-C connections under cyclic loading. The study takes into consideration.

The study is aimed at establishing the impact of thermal shock on the structural behavior of reinforced concrete B-C connections. As a result of the work carried out, the following tasks were solved: (1) the effect of the column axial load up to high levels (0, 25 %, 50 %, and 75 %), which is a parameter difficult to evaluate experimentally due to limitations in the loading machines and requirement of a special setup; (2) the significant reduction in strength and ductility of B-C connection due to thermal shock; (3) the impact of thermal shock on the lateral load capacities, net drifts, hysteresis loops, cracks distribution, energy dissipation, and failure modes. Eight NLFEA models were created, calibrated, and properly verified with the experimental results published by Shannag and Alhassan [1]. The actual loading setup, dimensions, reinforcement details, materials properties for the concrete and steel were considered in the NLFEA models.

2. Methods

ANSYS V16 software is an effective numerical method and important tool in the analysis of complex structures. The main benefits that NLFEA include: 1) substantial savings in the cost, time, and effort compared

with the fabrication and experimental testing of structure elements; 2) allows to change any parameter of interest to evaluate its influence on the structure, such as the concrete compressive strength; 3) allows to see the stress, strain, and displacement values at any location and at any load level. Eighteen full-scale models strengthened using CFRP are developed to carry out different investigated parameters.

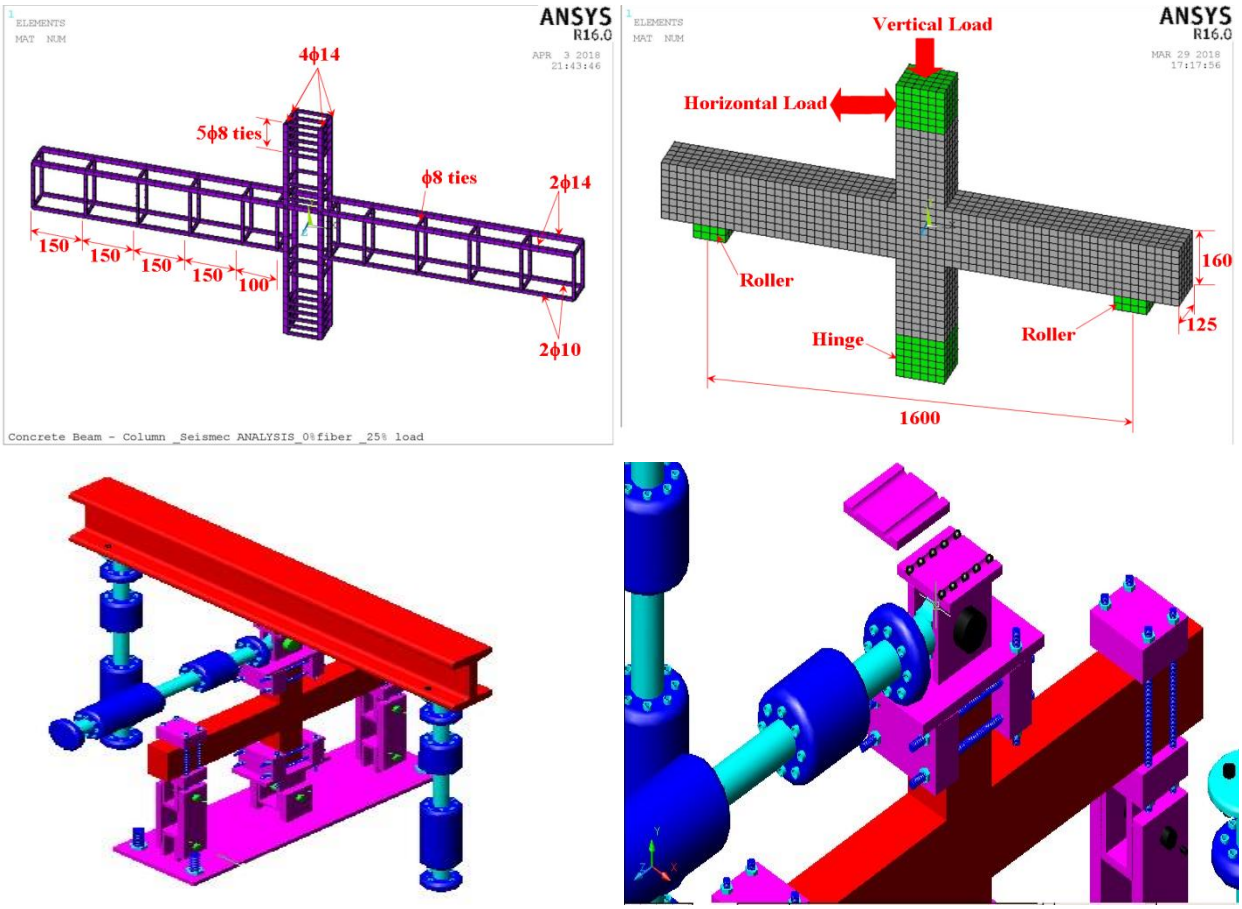

Figure 1. Specimen geometry, steel detailing, and schematic of applied loads setup (dimensions are in mm) [1].

2.1. Experimental Work Review

The validation process of the finite element model is based on the experimental work performed by Shannag and Alhassan [1]. The experimental work used in this paper was conducted by Shunnag and Alhassan [6] and the basic NLFEA models were calibrated based on that tested specimens. A total of ten nonlinear NLFEA models were created, calibrated, and properly verified with reputable experimental results, therefore the actual member's dimensions and reinforcement details as shown in Fig. 1. The column was rectangular with dimension 125×150 mm and 750 mm in cross-section and length, while the beam was rectangular with 200×125 mm and 1600 mm in cross section and length. The support was hinged at the bottom end of the column while kept free at the other end to allow for relative drift; simple rollers supported the beams-ends as shown in (Fig. 1).

2.2. Description of Non-linear Finite Element Analysis (NLFEA)

Concrete is non-homogenous and brittle material and has different behavior in tension and compression. SOLID 65 element is capable to predict the nonlinear behavior of concrete materials by using a smeared crack approach by ultimate uniaxial tensile and compressive strengths. The average compressive strength of the cylinders before and after being damaged by thermal shock were 25.8 and 10 MPa, respectively, and the average splitting tensile strength of the cylinders before and after being damaged by thermal shock were 3.1 and 0.7 MPa, respectively [41]. Poisson's ratio of 0.2 and shear transfer coefficient (β_t) of 0.2 for β_t was used in this study. Fig. 2(a) shows the stress-strain relationship for unconfined concrete which describes the post-peak stress-strain behavior.

LINK180 element was used to model the steel reinforcement. The 3-D spar element is a uniaxial tension-compression element with three degrees of freedom at each node with translations in the nodal x, y, and z directions. The element is also capable of plastic deformation. The steel in simulated models was assumed to be an elastic-perfectly plastic material and the same in compression and tension. There are two types of steel reinforcement in column, longitudinal bars (axial) with 14 mm-diameter and lateral bars (stirrups)

with 8 mm-diameter and spacing of 250 mm, and there are two types of steel reinforcement in beam, longitudinal bars (axial) with 14, 10 mm-diameter and lateral bars (stirrups) with 8 mm-diameter and spacing of 150 mm. Poisson's ratio of 0.3 and the yield stress of undamaged and damaged columns were 300 MPa and 0.78f_y [42], respectively, as well as the elastic modulus were 200 GPa and 0.6E_s [32], respectively, were used for the steel reinforcement. Fig. 2(b) shows the idealized stress-strain relationship. The steel plates were assumed to be linear elastic materials with a Poisson ratio and elastic modulus of 0.3 and 200 GPa, respectively.

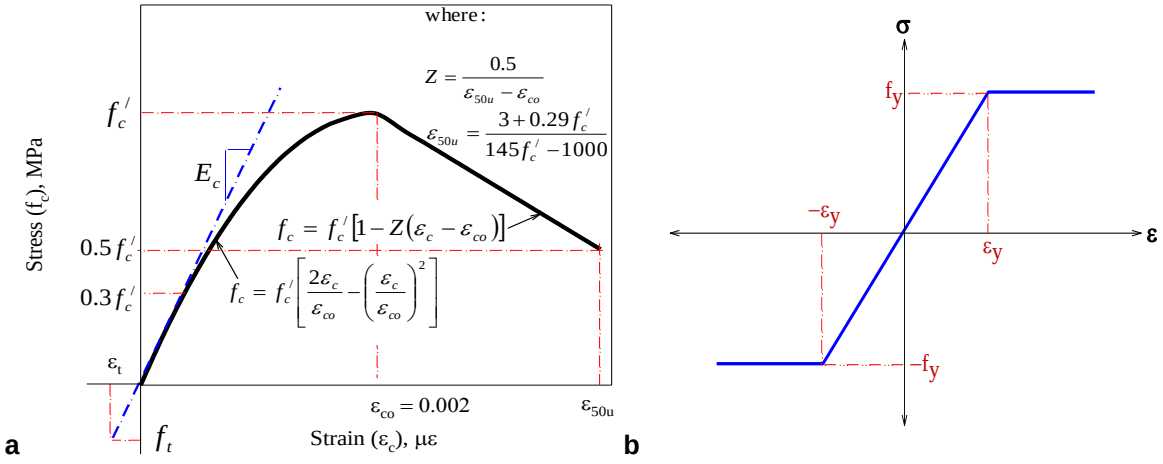

Figure 2. Stress-strain curves for: a. unconfined concrete [41] and b. steel reinforcement [42].

Table 1. Maximum loads and drifts under cyclic loading.

Group	Specimen	Axial load, %	Un-damaged/ Damaged	Maximum horizontal load, kN	Maximum horizontal net drift, mm
I	BC0J-UD	0	Un-damaged	14.5	7.67
	BC25J-UD	25		21.8	15.05
	BC50J-UD	50		26.2	22.51
	BC75J-UD	75		27.6	26.52
II	BC0J-D	0	Damaged	9.2 (0.63)	6.19 (0.81)
	BC25J-D	25		14.7 (0.67)	11.85 (0.79)
	BC50J-D	50		18.2 (0.69)	17.21 (0.76)
	BC75J-D	75		20.4 (0.74)	20.86 (0.74)

Note: C: Column, UD: un-damaged, D: Damaged

Full model was simulated to study the behavior of the control reinforced concrete B-C connection. The bond between the concrete and reinforcing bars was assumed to be perfect (no slippage). Also, full bond was assumed between the concrete and HPCJ to simulate strong contact interface, so coincide nodes were merged into single node with an appropriate tolerance. A convergence study was conducted to specify the optimum mesh size with 25 mm element meshing size as shown in Fig. 1. The boundary conditions at the two ends of the beam were constrained vertically $Uy = 0$, whereas the bottom end of the column was modeled as hinge support. The column axial load was applied at first loading step, and then the horizontal load was applied as displacement-controlled loading to ensure that the descending part of the load-displacement response curve is involved. This loading was applied incrementally to avoid sudden failure (solution divergence); the more the load sub-steps within a loading step, the more stable is the analysis process. ANSYS can automatically divide the loading into steps, but the number of sub-steps must be inserted manually. For each loading increment, the stiffness matrix of each element is updated each iteration to achieve the nonlinear response convergence using Newton-Raphson equilibrium iterative method with a tolerance of 0.001.

2.3. Investigated Parameters

The ANSYS program package was used to simulate the actual seismic structural behavior of the validated specimens as shown in Table 1. After that the simulated models were expanded to provide a parametric study in terms of the effect of column axial load level (0 %, 25 %, 50 %, and 75 %) and thermal shock damaged (un-damaged control B-C connection damaged B-C connection). A full description of the finite element modeling groups is shown in Table 1.

2.4. Validation Process

The basic NLFEA models were calibrated based on the tested specimens by Shannag and Alhassan [1] and therefore the actual members' dimensions and reinforcement details (Fig. 1) as well as materials properties for the concrete and steel (Fig. 2) were considered in the NLFEA models. Proper calibration was ensured using proper mesh size, boundary conditions, rate of loading, and considering materials' nonlinearities. Fig. 3 (top) shows the experimental load-drift hysteresis results for a virgin (top left) and strengthened (top right) B-C connections tested by Shannag and Alhassan [1]. Fig. 4 also shows the NLFEA results of this study for companion models. It can be clearly seen that the agreement is very good between the experimental and NLFEA results in terms of the ultimate load, ultimate drift, stiffness, degradation during the pushing and pulling stages of the loading. The cracking patterns, deformed shapes, and failure modes generated from the NLFEA were logical and in good agreement with the experimental results (Fig. 5).

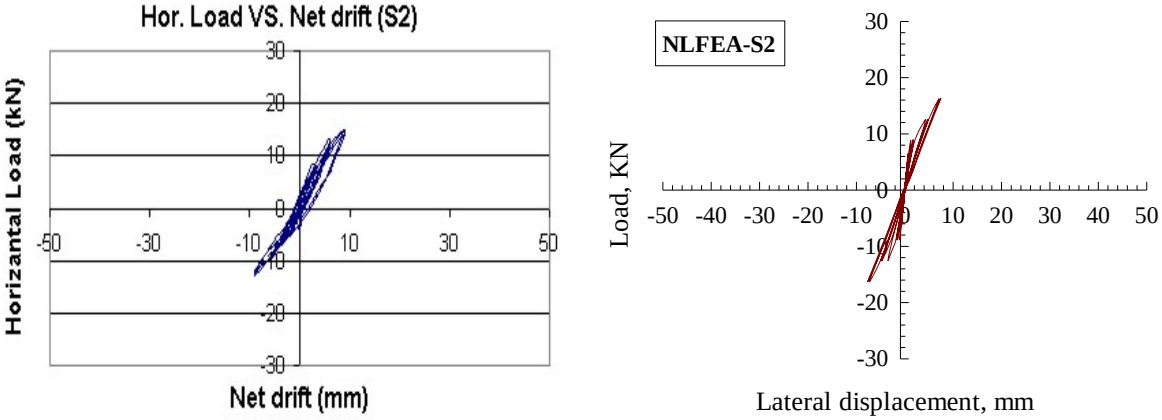

Figure 4. Validation of the NLFEA results with Shannag and Alhassan [1] results.

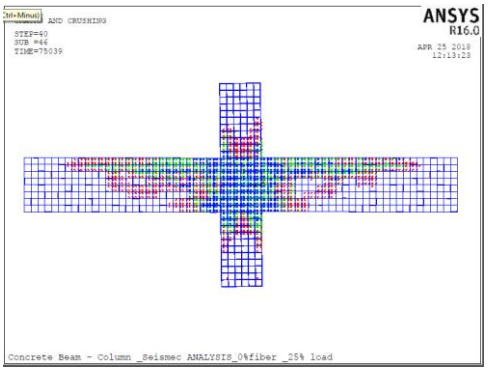

Figure 5. Typical cracks patterns.

3. Results and Discussion

3.1. Failure Mode

Fig. 5 shows the crack patterns and the brittle failure modes of the simulated beam-column connections. The first crack in control beam-column connection occurred in the top and the bottom of the diagonal joint area in the pushing part of the loading while in the pulling part crack begin to appear at the top and the bottom of the another diagonal side. Therefore, when the displacement increased the initial cracks extended from the joints side corner diagonally and also extended in the third direction due to the cyclic load that leads to open and closed these crack so for that reason the strength decreased. With further load increase, the cracks extended toward the beam and column and this caused a crushing failure in the concrete. Prior to failure, the control beam-column connection exhibited a yielding in the tension steel reinforcement at an ultimate horizontal load of 19.0 kN and the corresponding horizontal net drift of 9.1 mm. Fig. 6 shows the stress contours in the concrete and steel generated from ANSYS for each model. Comparing the stress contours for the specimens of each group show that as the column axial load increases, the intensity of the tensile stress within the joint area are is reduced and the yielding spreads more into the beam main steel. This indicates that the column axial load is advantageous for transforming the failure from brittle one in the joint into a ductile one in the beam, which reflects a strong column-weak beam action.

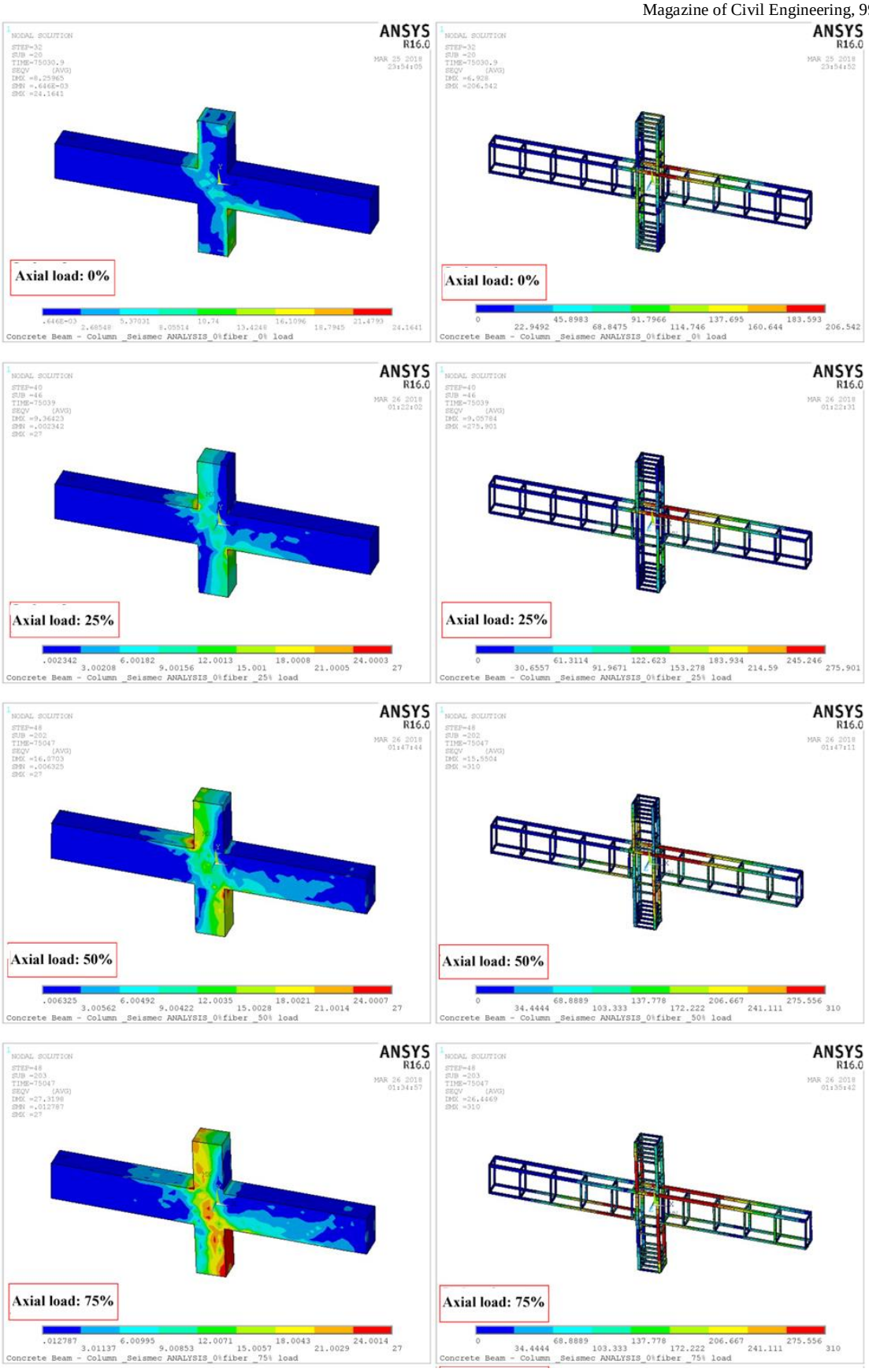

Figure 6. Typical Stress contours in concrete and steel.

3.2. Horizontal load-displacement hysteretic loops

The horizontal load-displacement hysteretic loops for all simulated B-C joints are shown in Fig. 7 (un-damaged) and Fig. 8 (Damaged). Inspection of Fig. 8 reveals that joint BC0J-D (axial load of 0 %, Damaged) exhibited minimum horizontal load and displacement. Joint BC0J-UD (axial load of 0 %, Un-damaged) (Fig. 7) exhibited higher strength and displacement than joint BC0J-D (Fig. 8) although the imposed

lateral reinforcement in these joint region is still inadequate to transmit the failure mechanism to the RC beam. Horizontal load-displacement loops of un-damaged joint show a considerable enhancement in the performance in terms of horizontal load and displacement (Fig. 7 and Fig. 8) because of the un-damaged system provided confinement to the joint rejoin by providing external cracks arresting mechanism and improving the post cracking ductility after reaching the ultimate load capacity and displacement. Also, the axial load level had a strong impact on the Horizontal load-displacement loops (Fig. 7 and Fig. 8) because the compressive stress in the column increased with the increasing of axial load which leads to the initiation of joint tensile concrete cracks that cause reduction in joint strength and maintaining the integrity of the joint connections.

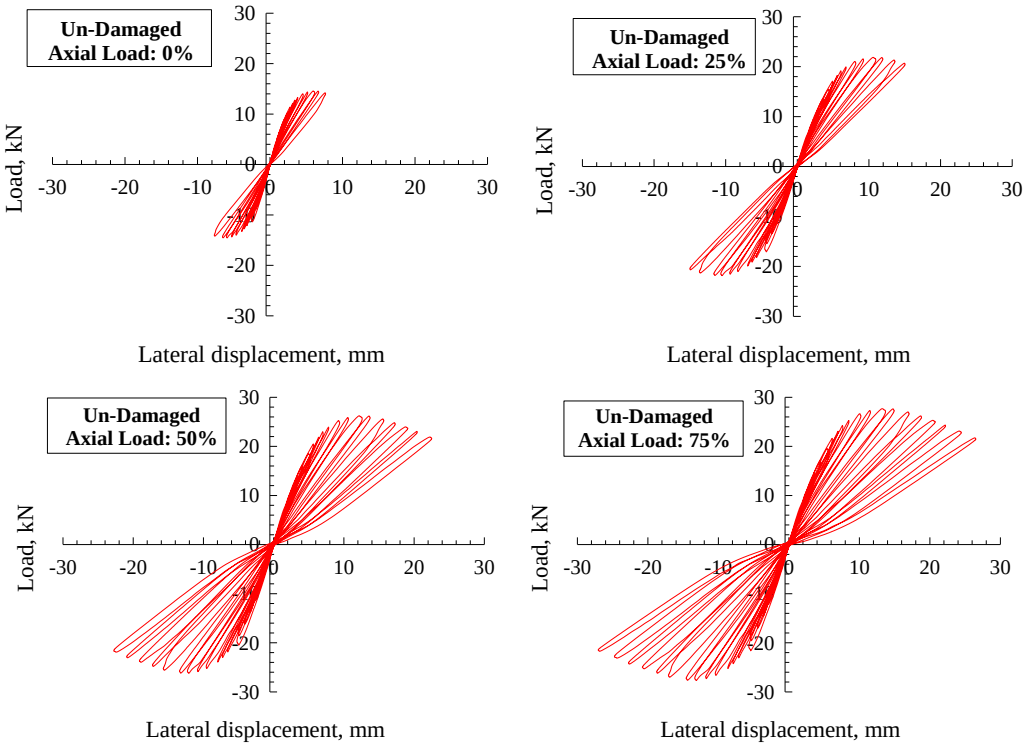

Figure 7. Horizontal load-net drift hysteresis loops for the un-damaged B-C connections.

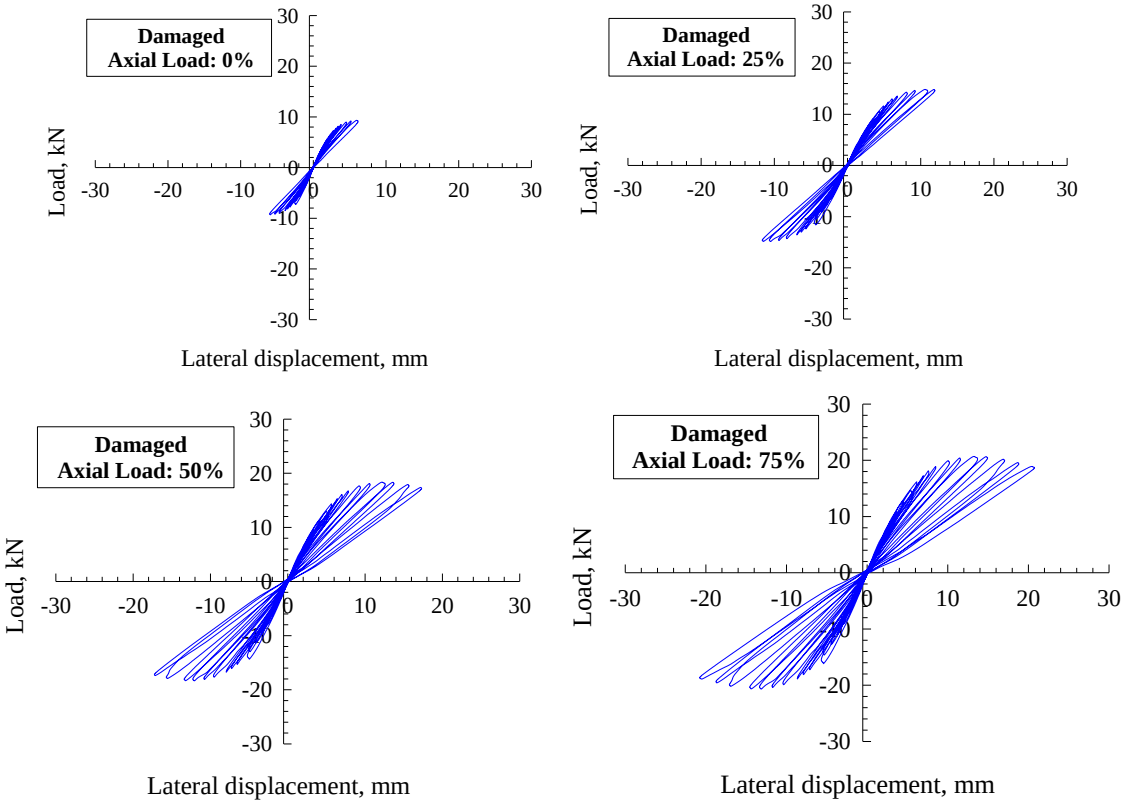

Figure 8. Horizontal load-net drift hysteresis loops for the damaged B-C connections.

3.3. Horizontal load-displacement envelopes

Fig. 9 shows the load-displacement envelopes for all simulated B-C joints were the maximum loads and corresponding displacements attained in each half cycle (pushing and pulling). Inspection of Fig. 9 reveals that the load and displacement increased with the increase of axial load percentage as well as the thermal shock had a helpful impact on both load and displacement.

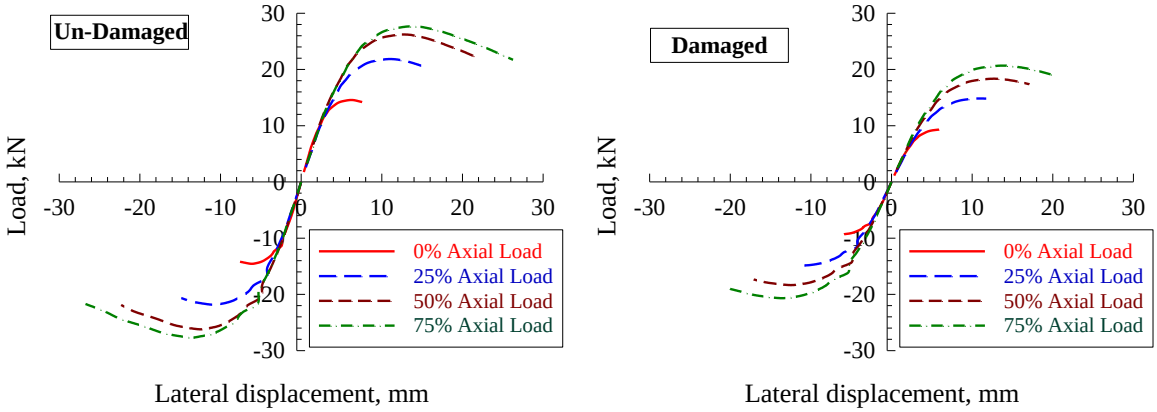

Figure 9. Horizontal load-displacement envelopes of B-C connections.

3.4. Ultimate horizontal load corresponding net drift displacement

The assessment of beams for horizontal load corresponding net drift displacement shows the excellent performance of B-C connections. For B-C connections, horizontal load corresponding net drift displacement can be related to the serviceability and ultimate load limit states, respectively, as shown in Table 1. The horizontal load corresponding net drift displacement percentages are defined as the horizontal load corresponding net drift displacement, respectively, of damaged B-C connections divided by the horizontal load corresponding net drift displacement, respectively, of damaged B-C connections as shown in Table 1. The drift displacement indicates how much the un-damaged B-C connections can sustain deformations without failure. Strength ratio also predicts the increase of load that the model can sustain.

Fig. 10 and 11 show the horizontal load corresponding net drift displacement with respect to un-damaged B-C connections, respectively, for all simulated models. Inspection of Fig. 10 reveals that the average enhancement percentage in horizontal load for the un-damaged is 50 %, 81 %, and 90 % for axial load of 25 %, 50 %, and 75 %, respectively. This reflected that the ultimate horizontal load increased with the increase of axial load percentages. Also, the average reduction percentage in horizontal load for the damaged with respect to un-damaged is 37 % is 33 %, 31 %, and 26 % for axial load of 0 %, 25 %, 50 %, and 75 %, respectively. Fig. 11 reveals that the average enhancement percentage in horizontal net drift for the un-damaged is 96 %, 193 %, and 245 % for axial load of 25 %, 50 %, and 75 %, respectively. Also, the average reduction percentage in horizontal net drift for the damaged with respect to un-damaged is 19 % is 21 %, 24 %, and 25 % for axial load of 0 %, 25 %, 50 %, and 75 %, respectively.

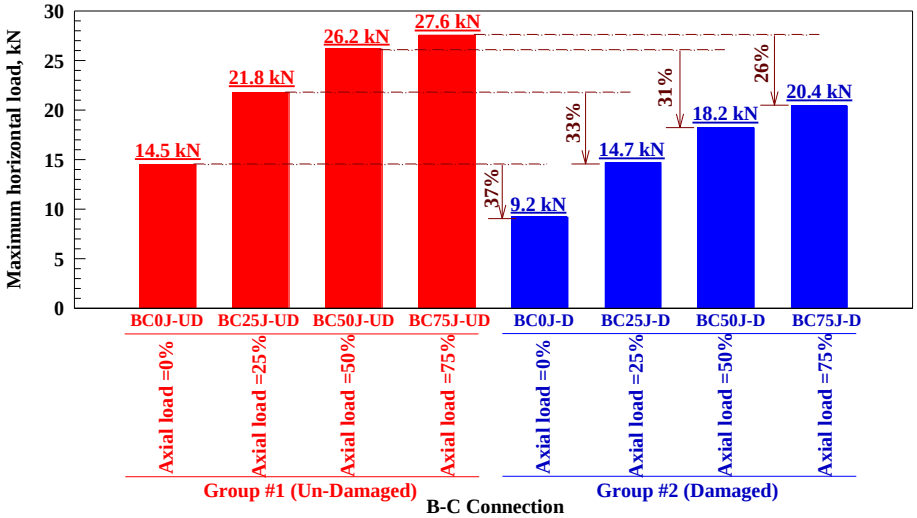

Figure 10. Ultimate horizontal load of B-C connections.

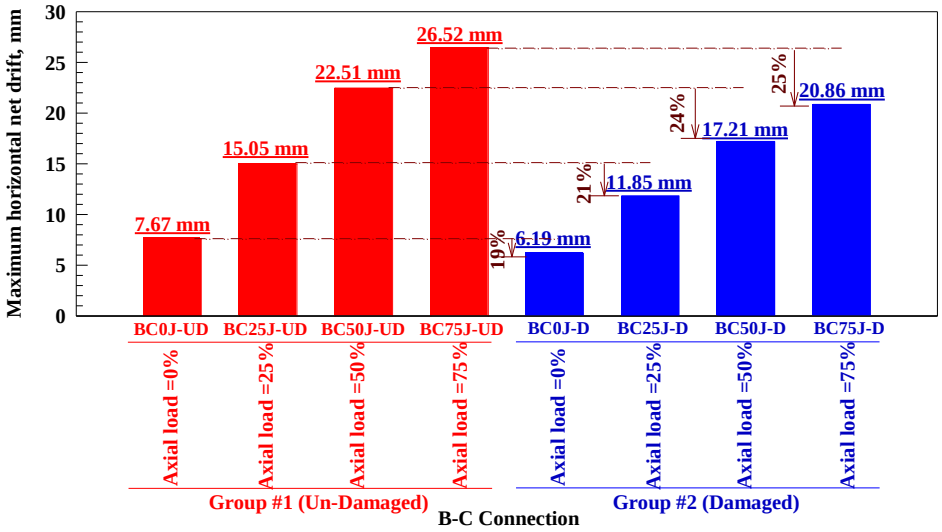

Figure 11. Ultimate horizontal net drift displacement of B-C connections.

3.5. The displacement ductility

The displacement ductility of the B-C connections was calculated from the ratio between the maximum and yield displacements (d_m/d_y). Table 2 shows the maximum and yield displacements which obtained from NLFEA results. Inspection of Table 2 reveals that the un-damaged connections BC0J-UD and BC25J-UD exhibited poor seismic performance and due to that the joint panel failed before the beam yielding of steel reinforcement. In contrast, BC50J-UD and BC75J-UD exhibited high displacement ductility values because of the excellent confinement to the joint-column region by higher axial load percentage which forced the joint to fail in a ductile behavior through formation of the plastic hinge in the beam. Also, Table 2 shows that the displacement ductility increased with the increased of axial load. While, all damaged connections exhibited poor seismic performance due to that the joint panel failed before the beam yielding of steel reinforcement.

Table 2. Displacement ductility values, energy dissipation, and steel strain.

Group	Specimen	Steel strain, $\mu\varepsilon$	Yield displacement d_y, mm	Maximum displacement d_m, mm	Displacement ductility d_m/d_y	Energy dissipation, kN.mm
I	BC0J-UD	916.75	Not yielded	7.29	NA	165
	BC25J-UD	1375.6	Not yielded	14.30	NA	498
	BC50J-UD	1651.1	2.636	21.39	8.5	918
	BC75J-UD	1742.3	2.164	25.19	12.3	1150
II	BC0J-D	601.35	Not yielded	5.86	NA	75
	BC25J-D	958.55	Not yielded	11.35	NA	250
	BC50J-D	1183.7	Not yielded	16.44	NA	481
	BC75J-D	1333.8	Not yielded	19.73	NA	654

Note: C: Column, UD: un-damaged, D: Damaged

3.6. Energy dissipation

The energy dissipation is defined as the area under the hysteretic loop for each cyclic load so when the building subjected to lateral loading a higher energy dissipation capability to absorb more energy. Fig. 12 shows the energy dissipation versus investigated parameter of simulated beam-column connections. Inspection of Fig. 12 reveals that the average enhancement percentage in energy dissipation for the un-damaged is 202 %, 458 %, and 598 % for axial load of 25 %, 50 %, and 75 %, respectively. This reflected that the energy dissipation increased with the increase of axial load percentages. Also, the average reduction percentage in energy dissipation for the damaged with respect to un-damaged is 46 % is 50 %, 53 %, and 57 % for axial load of 0 %, 25 %, 50 %, and 75 %, respectively.

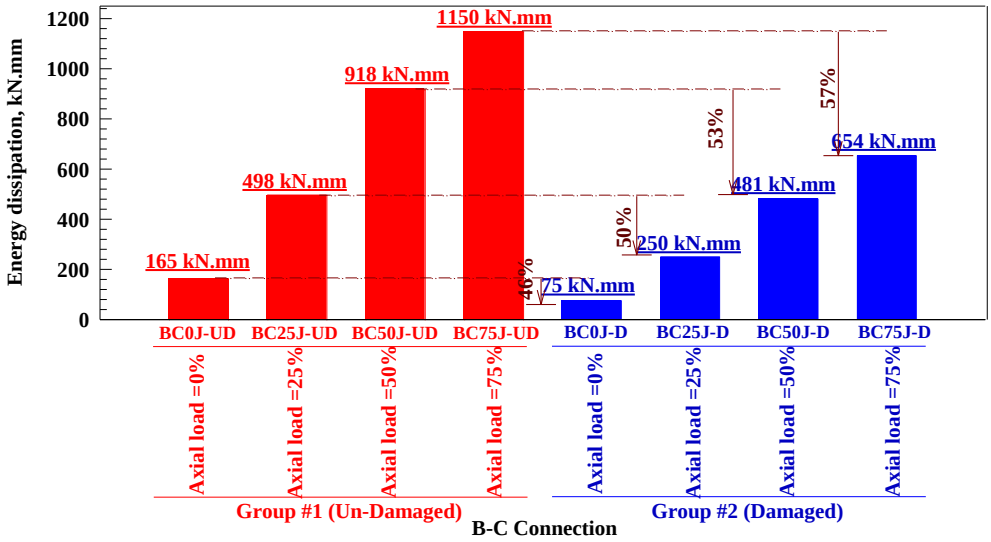

Figure 12. Energy dissipation of B-C connections.

3.7. Secant stiffness degradation

The secant stiffness degradation of the B-C connections is considered as a qualitative measure of the secant stiffness in each cycle. The method of stiffness degradation calculation involved: plotting the horizontal load-displacement hysteretic loops envelopes of each connection and then the secant stiffness for each cycle was calculated by dividing the summation of the maximum pushing and pulling loads on the summation of the maximum pushing and pulling corresponding displacements (the slope of the line between the maximum pulling and pushing and loads in each cycle) as shown in Fig. 13. Inspection of Fig. 13 reveals that the sharp reduction in secant stiffness values for damaged connections because the first crack initiated at initial stages of loading due to connection critical reinforcement details which caused concrete strength reduction and softening. While the stabilized reduction in secant stiffness values is clearly shown in un-damaged connections because the high strength concrete prevented the formation of main cracks to the joint-column region. Also, the un-damaged concrete considerably increased the initial secant stiffness of the connections and number of cycles. The effect of the column axial load percentage on increasing initial stiffness, stabilizing stiffness degradation, and increasing number of cycles is clear due to the increase in column compressive stress and reduces of the diagonal tensile stresses with the increasing of axial load. In addition, Fig. 13 shows that the secant stiffness degradation slightly increased when the axial load increased with a percentage of 4, 7, and 10 for axial load of 25 %, 50 %, and 75 %, respectively, with respect to un-damaged connection subjected to 0 % axial load. In addition, the thermal shock had an average reduction in the secant stiffness degradation of 39 %.

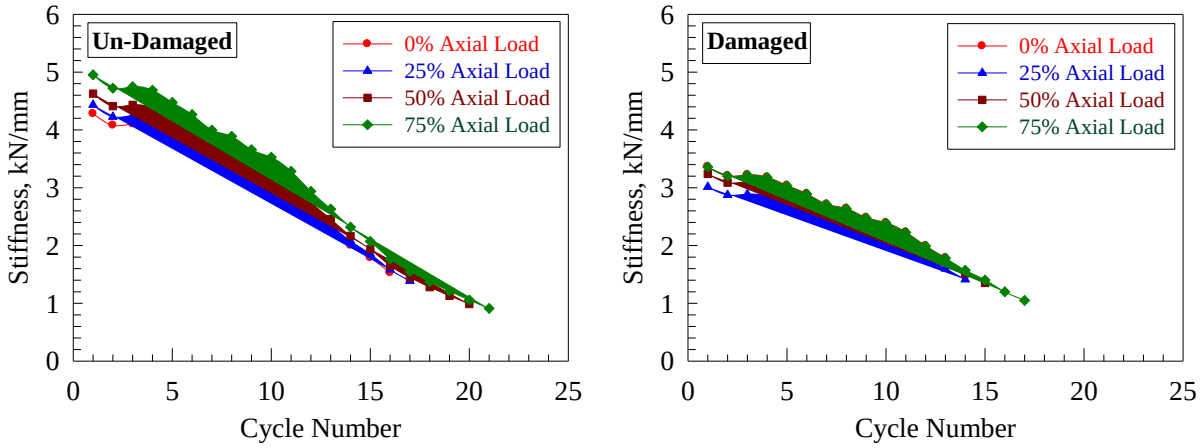

Figure 13. Secant stiffness degradation of simulated connection.

3.8. Comparison of NLFEA with other results

Comparison of NLFEA with Alhassan et al. [43], in virgin B-C connections, column axial load levels up to 75 % of its ultimate capacity were advantageous to its structural performance and substantially improve its lateral load capacity and ultimate net drift as a result of the induced axial compressive stresses in the joint region that alleviate the induced shear stresses by lateral loading which experienced similar behavior of NLFEA. The use of a higher axial load results in increase in the number of hysteresis loops indicating higher energy dissipation, enhanced ductility, and more stabilized stiffness degradation. The intensity of the stresses

within the joint decreases and yielding of steel spreads more to the beam main steel is almost the same performance as the NLFEA.

4. Conclusions

1. The performance of damaged beam-column connection was poor under cyclic loading simulating earthquake excitation, while the un-damaged beam-column connection had a significant enhancement on the seismic behavior of the weak connections. Higher horizontal load levels and larger horizontal drift displacements were attained and higher energy dissipation were achieved, and a significant increase in the joint strength was recorded.

2. In general, the higher axial load percentage results in increase in the number of hysteresis loops indicating higher energy dissipation, enhanced ductility, and more stabilized stiffness degradation. The intensity of the stresses within the joint decreases and yielding of steel spreads more to the beam main steel.

3. The energy of un-damaged beam-column connections could be dissipated by the joint before the system loses its stability as well as it is an indication of the joint maximum capacity to be stressed until failure.

4. Thermal shock has a significant impact on the behavior of beam-column connections. The increase in ductility is directly related to a decrease of compressive strength due to thermal shock.

References

1. Shannag, M., Alhassan, M. Seismic Upgrade of Interior Beam-Column Subassemblages with High-Performance Fiber Reinforced Concrete Jackets. ACI Structural Journal. 2005. 102(1). Pp. 131–138. DOI: 10.14359/13538
2. Shin, M., LaFave, J. Modeling of Cyclic Joint Shear Deformation Contributions in RC Beam-Column Connections to Overall Frame Behavior. Structural Engineering Mechanics. 2004. 18(5). Pp. 645–669. DOI: 10.12989/sem.2004.18.5.645
3. Ghobarah, A., Youssef, M. Modeling of RC Beam-Column Joints and Structural Walls. Journal of Earthquake Engineering. 2001. 5(1). Pp. 91–111. DOI: 10.1080/13632460109350387
4. Lowes, L., Altoontash, A. Modeling Reinforced Concrete Beam-Column Joints Subjected to Cyclic Loading. Journal of Structural Engineering. 2003. 129(12). Pp. 1686–97. DOI: 10.1061/(ASCE)0733-9445(2003)129:12(1686)
5. Mitra, N., Lowes LN. Evaluation, Calibration, and Verification of a Reinforced Concrete Beam-Column Joint Model. Journal of Structural Engineering. 2007. 133(1). Pp. 105–20. DOI: 10.1061/(ASCE)0733-9445(2007)133:1(105)
6. Venkatesan, B., Ilangovan, R., Jayabalan, P., Mahendran, N., Sakthieswaran, N. Finite Element Analysis (FEA) for the Beam-Column Joint Subjected to Cyclic Loading as Performed Using ANSYS. Circuits Systems. 2016. 7(1). Pp. 1581–1597. DOI: 10.4236/cs.2016.78138
7. Sasmal, S., Nath, D. Evaluation of Performance of Non-Invasive Upgrade Strategy for Beam–Column Sub-Assemblages of Poorly Designed Structures Under Seismic Type Loading. Earthquake Engineering Structural Dynamics. 2016. 45(1). Pp. 1817–1835. DOI: 10.1002/eqe.2730
8. Sasmal, S., Ramanjaneyulu, K., Novák, B., Lakshmanan, N. Analytical and Experimental Investigations on Seismic Performance of Exterior Beam–Column Sub- Assemblages of Existing RC-Framed Building. Earthquake Engineering Structural Dynamics. 2013. 42(1). Pp. 1785–1805. DOI: 10.1002/eqe.2298
9. Lima, C., Martinelli, E., Macorini, L., Izzuddin B. Modelling Beam-to-Column Joints in Seismic Analysis of RC Frames. Earthquakes Structures. 2017. 12(1). Pp. 119–133. DOI: 10.12989/eas.2017.12.1.119
10. Ibrahim, G., Shaaban, M. Finite element modeling of exterior beam-column joints strengthened by ferrocement under cyclic loading. Case Studies in Construction Materials. 2018. 8(1). Pp. 333–346. DOI: 10.1016/j.cscm.2018.02.010
11. Roy, B., Aminul, I. Cyclic Performance of Beam-Column Subassemblies with Construction Joint in Column Retrofitted with GFRP. Structures. 2018. 14(1). Pp. 290–300. DOI: 10.1016/j.istruc.2018.04.002
12. Marthong, C., Sangma, A., Choudhury, S., Pyrbot, R., Tron, S., Mawroh, L., Bharti, G. Structural Behavior of Recycled Aggregate Concrete Beam-Column Connection in Presence of Micro Concrete at Joint Region. Structures. 2017. 11(1). Pp. 243–251. DOI: 10.1016/j.istruc.2017.07.001
13. Marthong, C., Marthong, S. An experimental study on the Effect of PET Fibers on the Behavior of Exterior RC Beam-Column Connection Subjected to Reversed Cyclic Loading. Structures. 2016. 5(1). Pp. 175–185. DOI: 10.1016/j.istruc.2015.11.003
14. Baji, H., Eslami, A., Ronagh, H. Development of a Nonlinear FE Modelling Approach for FRP-Strengthened RC Beam-Column Connections. Structures. 2015. 3(1). Pp. 272–281. DOI: 10.1016/j.istruc.2015.06.003
15. Kodur, V., Agrawal, A. An approach for evaluating residual capacity of reinforced concrete beams exposed to fire. Engineering Structures. 2016. 110(1). Pp. 293–306. DOI: 10.1016/j.engstruct.2015.11.047
16. Al-Ostaz, A., Irshidat, M., Tenkhoff, B., Ponnapalli, P. Deterioration of bond integrity between repair material and concrete due to thermal and mechanical incompatibilities. Journal of Materials in Civil Engineering. 2010. 22(2). Pp. 136–144. DOI: 10.1061/(ASCE)0899-1561(2010) 22:2(136).
17. Nedviga, E., Beresneva, N., Gravit, M., Blagodatskaya, A. Fire Resistance of Prefabricated Monolithic Reinforced Concrete Slabs of “Marko” Technology. Adv. Intell. Syst. Comput. 2018. 692(1). Pp. 739–749. DOI: 10.1007/978-3-319-70987-1_78
18. Hezhev, T., Zhurtov, A., Tsipinov, A., Klyuev, S. Fire resistant fibre reinforced vermiculite concrete with volcanic application. Mag. Civ. Eng. 2018. 80(1). Pp. 181–194. DOI: 10.18720/MCE.80.16
19. Goremikins, V., Blesak, L., Novak, J., Wald, F. Experimental investigation on SFRC behaviour under elevated temperature. J. Struct. Fire Eng. 2017. 8(1). Pp. 287–299. DOI: 10.1108/JSFE-05-2017-0034
20. Purkiss, J. Steel fibre reinforced concrete at elevated temperatures. International Journal of Cement Composites and Lightweight Concrete. 1984. 6(3). Pp. 179–184. DOI: 10.1016/0262-5075(84)90006-X. DOI: 10.14311/asfe.2015.055
21. Blesak, L., Goremikins, V., Wald, F., Sajdlova, T. Constitutive model of steel fibre reinforced concrete subjected to high temperatures. Acta Polytech. 2016. 56(1). Pp. 417–424. DOI: 10.14311/AP.2016.56.0417

22. Korsun, V., Vatin, N., Franchi, A., Korsun, A., Crespi, P., Mashtaler, S. The strength and strain of high-strength concrete elements with confinement and steel fiber reinforcement including the conditions of the effect of elevated temperatures. Procedia Eng. 2015. 117(1). Pp. 970–979. DOI: 10.1016/j.proeng.2015.08.192
23. Goremikins, V., Blesak, L., Novak, J., Wald, F. Experimental method on investigation of fibre reinforced concrete at elevated temperatures. Acta Polytech. 2016. 56(1). Pp. 258–264. DOI: 10.14311/AP.2016.56.0258
24. Selyaev, V., Nizina, T., Balykov, A., Nizin, D., Balbalin, A. Fractal analysis of deformation curves of fiber-reinforced fine-grained concretes under compression. PNRPU Mech. Bull. 2016. 1(1). Pp. 129–146. DOI: 10.15593/perm.mech/2016.1.09
25. Petr Bílý, Alena Kohoutková. A Numerical Analysis of the Stress-strain Behavior of Anchorage Elements and Steel Liner of a Prestressed Concrete Containment Wall. Structures. 2017. 12(1). Pp. 24–39. DOI: 10.1016/j.istruc.2017.07.003
26. Bílý, P., Kohoutková, A. Sensitivity analysis of numerical model of prestressed concrete containment. Nucl. Eng. Des. 2015. 295(1). Pp. 204–214. DOI: 10.1016/j.nucengdes.2015.09.027
27. Al-Rousan, R. Behavior of two-way slabs subjected to drop-weight. Magazine of Civil Engineering. 2019. 90(6). Pp. 62–71. DOI: 10.18720/MCE.90.6
28. Al-Rousan, R. The impact of cable spacing on the behavior of cable-stayed bridges. Magazine of Civil Engineering. 2019. 91(7). Pp. 49–59. DOI: 10.18720/MCE.91.5
29. Krishan, A., Rimshin, V., Erofeev, V., Kurbatov, V., Markov, S. The energy integrity resistance to the destruction of the long-term strength concrete. Procedia Eng. 2015. 117(1). Pp. 211–217. DOI: 10.1016/j.proeng.2015.08.143
30. Hyo-Gyoung, Kwak, Jae, Hong Kim. Numerical models for prestressing tendons in containment structures. Nuclear Engineering and Design. 2006. 236(1). Pp. 1061–1080. DOI: 10.1016/j.nucengdes.2005.10.010
31. Korsun, V., Vatin, N., Korsun, A., Nemova, D. Physical-mechanical properties of the modified fine-grained concrete subjected to thermal effects up to 200°S. Appl. Mech. Mater. 2014. 633–634. Pp. 1013–1017. DOI: 10.4028/www.scientific.net/AMM.633-634.1013
32. Korsun, V., Korsun, A., Volkov, A. Characteristics of mechanical and rheological properties of concrete under heating conditions up to 200°C. MATEC Web Conf. 2013. 6(1). Pp. 07002. DOI: 10.1051/matecconf/20130607002
33. Petkova, D., Donchev. T., Wen. J. Experimental study of the performance of CFRP strengthened small scale beams after heating to high temperatures. Construction and Building Materials. 2014. 68(1): Pp. 55–61. DOI: 10.1016/j.conbuildmat.2014.06.014
34. Ji, G., Li, G., Alaywan, W. A new fire resistant FRP for externally bonded concrete repair. Construction and Building Materials. 2013. 42(1). Pp. 87–96. DOI: 10.1016/j.conbuildmat.2013.01.008
35. Trentin, C., Casas, J. Safety factors for CFRP strengthening in bending of reinforced concrete bridges. Composite Structures. 2015. 128(1). Pp. 188–198. DOI: 10.1016/j.compstruct.2015.03.048
36. Ferrari, V., Hanai, J., Souza, R. Flexural strengthening of reinforcement concrete beams using high performance fiber reinforcement cement-based composite (HPFRCC) and carbon fiber reinforced polymers (CFRP). Construction and Building Materials. 2013. 48(1). Pp. 485–498. DOI: 10.1016/j.conbuildmat.2013.07.026
37. Attari, N., Amziane, S., Chemrouk, M. Flexural strengthening of concrete beams using CFRP, GFRP and hybrid FRP sheets. Construction and Building Materials. 2012. 37(1). Pp. 746– 757. DOI: 10.1016/j.conbuildmat.2012.07.052
38. Kara, I., Ashour, A., Körog˘lu, M. Flexural behavior of hybrid FRP/steel reinforced concrete beams. Composite Structures. 2015. 129(1). Pp. 111–121. DOI: 10.1016/j.compstruct.2015.03.073
39. Kolchunov, V., Dem'yanov, A. The modeling method of discrete cracks in reinforced concrete under the torsion with bending. Magazine of Civil Engineering. 2018. 81(5). Pp. 160–173. DOI: 10.18720/MCE.81.16
40. Travush, V., Konin, D., Krylov, A. Strength of reinforced concrete beams of high-performance concrete and fiber reinforced concrete. Magazine of Civil Engineering. 2018. No. 77(1). Pp. 90–100. DOI: 10.18720/MCE.77.8
41. Al-Rousan, R. Behavior of CFRP Strengthened Columns Damaged by Thermal Shock. Magazine of Civil Engineering. 2020. 95(3). Pp. 48–62. DOI: 10.18720/MCE.95.3
42. Zhang, YX, Bradford, MA. Nonlinear analysis of moderately thick reinforced concrete slabs at elevated temperatures using a rectangular layered plate element with Timoshenko beam functions. Engineering Structures. 2007. 29(10). Pp. 2751–2761. DOI: 10.1016/j.engstruct.2007.01.016
43. Alhassan, MA, Al-Rousan, RZ, Amaireh, LK, Barfed, MH. Nonlinear Finite Element Analysis of B-C Connections: Influence of the Column Axial Load, Jacket Thickness, and Fiber Dosage. Structures. 2018. 16(1). Pp. 50–62. DOI: 10.1016/j.istruc.2018.08.011

Contacts:

Rajai Al-Rousan, rzalrousan@just.edu.jo